Optimal Perturbations in the Eady Model: Resonance versus PV Unshielding

H. DE VRIES

Institute for Marine and Atmospheric Research Utrecht, Utrecht University, Utrecht, Netherlands

J. D. OPSTEEGH

Royal Netherlands Meteorological Institute, De Bilt, Netherlands

(Manuscript received 4 March 2004, in final form 3 August 2004)

ABSTRACT

Using a nonmodal decomposition technique based on the potential vorticity (PV) perspective, the optimal perturbation or singular vector (SV) of the Eady model without upper rigid lid is studied for a kinetic energy norm. Special emphasis is put on the role of the continuum modes (CMs) in the structure of the SV, and on the importance of resonance to the SV evolution. The basis for the SV is formed by a number of nonmodal structures, each consisting of a superposition of one CM and one edge wave, such that the initial surface potential temperature (PT) is zero. These nonmodal structures are used as PV building blocks to construct the SV. The motivation for using a nonmodal approach is that no attempt has been made so far to include the CM residing at the steering level of the surface edge wave in the perturbation, although it is known that this CM is in linear resonance with the surface edge wave.

Experiments with one PV building block in the initial disturbance show that the SV growth is dominated by the resonance effect except for small optimization times (less than 1 day), in which case the unshielding of PV and surface PT dominates the growth of the SV. The PV–PT unshielding provides additional growth to the SV and this explains the observation that the PV resides above the resonant level.

More PV building blocks are added to include PV unshielding as a third growth mechanism. Which of the three mechanisms dominates during the SV evolution depends on the region of interest (interior or surface), as well as on the optimization time and on the number of building blocks used. At the surface, resonance plays a dominant role even when a large number of building blocks is used and relatively small optimization times are used. For the interior of the domain, PV unshielding becomes the dominant growth mechanism when more than two PV building blocks are used. With increasing optimization times, the PV distribution of the SV becomes increasingly more concentrated near the steering level of the edge wave. This concentration of PV is explained by the enhanced importance of resonance for long optimization times as compared to short optimization times.

1. Introduction

For more than a century there has been interest in extratropical surface cyclogenesis and its underlying dynamics. Eady (1949) examined the stability of a basic state corresponding approximately with the observed mean flow at midlatitudes. The basic state is formed by an inviscid shear flow between two horizontal rigid lids representing the earth surface and the tropopause. Eady solved the linear stability problem for this basic state and obtained the dispersion relation for the two discrete normal modes that are characterized by nonzero perturbation potential temperature (PT) and zero interior perturbation quasigeostrophic potential vorticity (PV). These normal modes are unstable if their horizontal wave number is smaller than a critical value. The unstable normal mode solutions have a number of remarkable similarities with observed growing extratropical cyclones.

Ever since the pioneering work of Eady, researchers have looked for different growth mechanisms to explain the observed behavior of developing cyclones. Pedlosky (1964) solved the initial value problem for the Eady model in complete generality and showed that there is another class of disturbance structures supported by the background flow. These so-called continuum modes (CMs) are characterized by both a singular perturbation of PV at some interior level and a nonzero potential temperature structure at the boundaries. It is only with the help of this infinite number of CMs that the finite-time dynamics of an arbitrary initial disturbance is represented correctly in the Eady model. The observation that transient effects of superposition

Corresponding author address: H. de Vries, Institute for Marine and Atmospheric Research Utrecht, Utrecht University, Utrecht, Netherlands.
E-mail: H.deVries@phys.uu.nl

can result in remarkable perturbation growth is not new and dates back to the work of Orr (1907). Farrell (1982, 1984, 1988, 1989) has been among the first to explicitly show that the CMs can play an important role in the cyclogenesis problem. The basic question Farrell addressed is the following: What is the structure of the initial perturbation, such that for a given basic state the perturbation linearly amplifies most rapidly for a given norm over a prescribed time interval? These optimal perturbations are called singular vectors (SVs). Farrell showed that the finite-time rapid baroclinic amplification of a favorably configured initial disturbance can exceed the growth due to normal mode instability. While eventually the growing normal mode becomes important, the initial growth of the SV is dominated by what is called nonmodal wave growth. Here, a nonmodal disturbance is defined as any disturbance structure that comprises more than one single normal mode (Farrell 1984). On a weather map the SV appears as a localized structure. The SV gives an indication of the location where future development can be expected, and where forecast errors may grow rapidly. Because of this signaling function, it is worthwhile to understand the SV in terms of the underlying dynamics.

Most analytical studies on singular vectors for the Eady model concentrate on the growing normal modes and do not consider the CMs. Rotunno and Fantini (1989) studied optimal perturbations created by the superposition of growing normal modes of one fixed wavelength. Their analytical work has been extended to include variable wavenumbers by Fischer (1998).

Much less is known about the fact that the CM can generate sustained perturbation growth as well. If the PV of a CM is located exactly at the steering level of one of the edge waves, an edge wave is resonantly excited and the perturbation streamfunction grows linearly in time. The existence of a linear resonance has been found before in analytical studies of the Eady model where the upper rigid lid was removed (Thorncroft and Hoskins 1990; Chang 1992; Davies and Bishop 1994; Bishop and Heifetz 2000) but no serious attempt has been made so far to include the impact of the linear resonance in an analytical approach to the SV. To fill the gap we will concentrate on the role of the CMs in the SV structure and especially on the importance of resonance in the SV evolution. This is done using an analytical treatment of the semi-infinite Eady model. The results will be compared with the existing literature on shortwave numerical SV analyses, to be summarized below.

Although the CM is ignored in the analytical studies, the CMs have been included in most numerical approaches. Farrell (1988) was the first to calculate the SV for simplified atmospheric models using streamfunction variance (L2) and total kinetic energy as a norm. He found optimal perturbations that have a PV distribution which initially tilt extremely upshear with height. These results were confirmed and worked out for the Eady model in more detail by Mukougawa and Ikeda (1994). Hakim (2000) studied the evolution of an upper-level PV anomaly and found that the growth due to unstable normal modes is more important than SV growth. Similarly, Badger and Hoskins (2001) studied the dynamics of a spatially localized vortex but they noticed that PV unshielding plays an important role in the initial stage of the development. The effect of growth due to linear resonance is not explicitly considered in these numerical studies. The CM can only yield linear resonance in the Eady model if the wavenumber of the perturbation is large enough to guarantee a steering level within the flow domain. Let us therefore focus on the shortwave SVs in the numerical approaches to the SV in the Eady model.

Morgan (2001) and Morgan and Chen (2002) have analyzed the Eady model SV (calculated with modal analysis) for the L2-norm using two different numerical partitionings of the SV. First they use a modal partitioning. The SV streamfunction ψ_{sv} is divided into an Eady edge wave part, ψ_{nm} and a CM part ψ_{cm}. The advantage of such a partitioning is clear. Modal solutions do not change their structure with time. However, there is also a disadvantage. As a result of the necessary constraints at horizontal rigid surfaces, the streamfunction of the CM becomes nearly singular if the PV is located near the steering level of the neutral edge wave, which makes it difficult to address the optimization problem numerically. This may be a motivation for choosing a PV partitioning to determine the SV. Morgan and Chen (2002) chose this PV partitioning to get a better understanding of the SV. In the PV-based partitioning, one decomposes the streamfunction into an interior PV part ψ_{pv} with zero boundary PT, and a part ψ_{θ} associated with PT at the boundaries but zero interior PV. The advantage of this approach is that it is physically transparent. However, the individual parts now evolve in a nonmodal way, which may be a disadvantage for a clear understanding.

Morgan (2001) analyzed the shortwave SV evolution and this resulted in the following schematic three-stage development: 1) a superposition of interior PV anomalies, 2) a subsequent intensification of the boundary potential temperature anomalies due to the advection of background potential temperature gradient by the winds associated with interior PV, and 3) finally a transient interaction between the upper and lower boundary potential temperature anomalies. The observations of Morgan (2001) have been analyzed and confirmed by Morgan and Chen (2002). They confirm the important role of initial masking and subsequent unshielding of the Eady edge modes by the CMs in the evolution of the SV. They observe that for the shortwave perturbations, only a small number of CMs are required to mask the edge modes.

The work of Morgan (2001) and Morgan and Chen (2002) has been generalized and reconsidered by Kim and Morgan (2002) using both a total quasigeostrophic

energy norm and a potential enstrophy norm. From their work, it can be concluded that the choice of norm may substantially influence the result. It depends on the specific choice of which stage of the aforementioned three-stage SV evolution dominates. Furthermore, in Morgan and Chen (2002) and Kim and Morgan (2002) the length of the optimization time is varied and it is found that for increasing optimization time, the importance of the PV near the steering levels of the edge waves becomes more important for shortwave perturbations. The explanation they give for this PV concentration is that it allows for a longer near-resonant interaction between the PV and the edge wave.

In the present paper we will investigate the structure of the SV of the Eady model with an emphasis on the importance of the effects of resonance and PV unshielding. In order to extend the existing literature on analytically constructed optimal perturbations (Rotunno and Fantini 1989; Fischer 1998), we will retain the CMs. To quantify the importance of resonance for the surface dynamics, we use the semi-infinite version of the Eady model as formulated by Thorncroft and Hoskins (1990). The surface dynamics of this model resemble the surface dynamics of the conventional Eady model above the instability cutoff. Section 2 introduces the semi-infinite version of the Eady model with special emphasis on the continuous spectrum. In section 3 a PV basis is constructed with the help of nonmodal structures. These nonmodal structures consist of a superposition of one CM and one edge wave such that initially the surface potential temperature is zero. The nonmodal structures are used as PV building blocks to construct the SV. In section 4 we start with the optimal position for one PV building block. In section 5 the generalization toward a general distribution of PV is considered. Section 6 consists of a summary of the main conclusions and finally two appendices are added to clarify some points concerning numerical techniques.

2. Equations and normal mode solutions

The basic equation that governs the dynamics of the Eady model without upper rigid lid is the conservation of quasigeostrophic PV q

$$\left(\frac{\partial}{\partial t} + \overline{U}\frac{\partial}{\partial x}\right) q(x, y, z, t) = 0, \tag{2.1}$$

where $\overline{U} = \Lambda z$ is the basic zonal flow, y the meridional direction, x the zonal direction, z the vertical direction, and t time. The basic state is assumed to have zero interior PV and Λ has a typical value of 3 m s^{-1} per kilometer height, which is characteristic for the midlatitudes. Also, q is related to the perturbation streamfunction ψ by:

$$q(x, y, z, t) = \left(\frac{\partial^2}{\partial x} + \frac{\partial^2}{\partial y} + \frac{1}{S^2}\frac{\partial^2}{\partial z^2}\right)\psi(x, y, z, t), \tag{2.2}$$

with $S^2 = (N_0 H)^2 (f_0 L)^{-2}$ as the the stratification parameter or Burger number, which in the present study is kept at unity, $S^2 = 1$. Variables have been nondimensionalized using the scalings (L, H, L/U, $f_0 LU$) where $L = N_0 H / f_0 \sim 10^6$ m scales the horizontal coordinates x and y, and $H \sim 10^4$ m scales the vertical coordinate z. Here, $L/U \sim 9.26$ h is the characteristic time scale, and $f_0 LU \sim 3.10^3$ m^2 s^{-2} scales the geostrophic streamfunction. Furthermore, $U \sim 30$ m s^{-1}. Finally a constant Coriolis parameter $f_0 \sim 10^{-4}$ s^{-1} is assumed as well as a constant Brunt–Väisälä (buoyancy) frequency $N_0^2 \sim 10^{-4}$ s^{-2}. Wavenumbers of the perturbations have been nondimensionalized in a similar way. A nondimensional zonal wavenumber $k = 1$ corresponds with a physical wavelength of 6280 km.

At the earth surface the condition that the vertical velocity equals zero leads to

$$\left(\frac{\partial}{\partial t} + \overline{U}\frac{\partial}{\partial x}\right)\frac{\partial \psi}{\partial z} - \frac{\partial \overline{U}}{\partial z}\frac{\partial \psi}{\partial x} = 0 \quad (z = 0), \tag{2.3}$$

where $\partial\psi/\partial z \equiv \theta$ defines the PT. As a scaling for PT, we choose $(ULf_0 g^{-1} H^{-1})\Theta_{00} = 9.18$ K, for a given reference potential temperature $\Theta_{00} = 300$ K and $g = 9.81$ m s^{-2} the gravity constant. For consistency, it is required that the perturbation streamfunction vanishes at infinite height. Because $\overline{U} = 0$ at the earth surface, (2.3) implies an exact balance between the tendency of the local perturbation potential temperature $\partial\theta/\partial t$ and the horizontal advection of mean temperature by the perturbation meridional velocity $\Lambda\partial\psi/\partial x$. This balance will have a important effect in the structure of the CM to be discussed later.

At the channel walls the meridional velocity $v = \partial\psi/\partial x$ vanishes. For simplicity we have chosen to study perturbations that are homogeneous in the meridional direction. If the meridional wavenumber is nonzero, the numerical growth values obtained in the experiments to be discussed later will change. However, it is to be expected that the results do not change qualitatively, because the growth mechanisms available to the system remain the same.

a. Edge waves

Modal solutions for the Eady model without an upper rigid lid appear in two classes: with and without interior PV. We treat them separately because of the differences in vertical structure. Solving (2.1) and (2.3) for $q = 0$ one obtains the streamfunction of the Eady edge wave

$$\psi^{\mathrm{nm}}(x, z, t) = e^{-\mu z} \sin\left[k\left(x - \frac{\Lambda}{\mu}t\right)\right], \tag{2.4}$$

where $\mu = S(k^2 + l^2)^{1/2} = 1/H_R$ defines the inverse Rossby height. Due to the absence of the upper rigid boundary, the Charney–Stern condition for instability is not satisfied and the solution is a baroclinically stable

oscillation that propagates zonally with the speed of the basic-state flow at one Rossby height above the surface.

b. Continuum modes

The semi-infinite Eady model contains an infinite number of neutral normal modes, called CMs. These modes have nonzero PV at some interior level h,

$$q(x, z, t) = Q\delta(z - h)\sin[k(x - \Lambda ht)], \qquad (2.5)$$

with Q being the amplitude of PV. Notice that $q(x, z, t) = q(x - \Lambda ht, z, 0)$ due to PV conservation. Thorncroft and Hoskins (1990) calculated the streamfunction of the CM. For $h \neq 1/\mu$, they obtained

$$\psi^{\mathrm{cm}}(x, z, t) = \underbrace{\frac{Q}{\mu}[H(z - h)\sinh \mu(z - h) - e^{-\mu h}\cosh \mu z]\sin[k(x - \Lambda ht)]}_{\psi^{\mathrm{cm}}_{\mathrm{pv}}(x,z,t)} + \underbrace{\frac{Q}{\mu}\left(\frac{e^{-\mu h}}{1 - \mu h}\right)e^{-\mu z}\sin[k(x - \Lambda ht)]}_{\psi^{\mathrm{cm}}_{\theta}(x,z,t)}, \qquad (2.6)$$

where $H(z-h)$ is the Heavyside step function.[1] We have partitioned the streamfunction ψ^{cm} into a PT part $\psi^{\mathrm{cm}}_{\theta}$ and a PV part $\psi^{\mathrm{cm}}_{\mathrm{pv}}$ such that $\psi^{\mathrm{cm}} = \psi^{\mathrm{cm}}_{\theta} + \psi^{\mathrm{cm}}_{\mathrm{pv}}$. In this PV partitioning, $\psi^{\mathrm{cm}}_{\theta}$ is associated with anomalous surface PT only and not with interior PV. To the contrary, $\psi^{\mathrm{cm}}_{\mathrm{pv}}$ has zero surface PT, but nonzero interior PV. This decomposition is due to Morgan and Chen (2002) and will be used throughout the paper:

$$\left(\frac{\partial^2}{\partial z^2} - \mu^2\right)\psi_{\mathrm{pv}} = q, \quad \left(\frac{\partial \psi_{\mathrm{pv}}}{\partial z}\right)\bigg|_{z=0} = 0, \qquad (2.7)$$

$$\left(\frac{\partial^2}{\partial z^2} - \mu^2\right)\psi_{\theta} = 0, \quad \left(\frac{\partial \psi_{\theta}}{\partial z}\right)\bigg|_{z=0} = \theta|_{z=0}. \qquad (2.8)$$

Observing (2.6), it is immediately clear that the temperature part $\psi^{\mathrm{cm}}_{\theta}$ in (2.6) has the same vertical structure as the edge wave (2.4) although it propagates with a different speed. Furthermore, the amplitude of $\psi^{\mathrm{cm}}_{\theta}$ becomes arbitrarily large when h approaches the steering level of the neutral edge wave. Figure 1 shows the PT structure of a CM for various values of the height h of the (positive amplitude) PV. This figure shows that a CM located above $1/\mu$ has a warm-surface PT. Contrast this with the CM below $h = 1/\mu$, which has a cold-surface PT. Sign and amplitude of $\psi^{\mathrm{cm}}_{\theta}$ at the surface depend on the height of the PV anomaly. This follows directly from the thermodynamic equation (2.3). In terms of the PV partitioning (2.3) reads

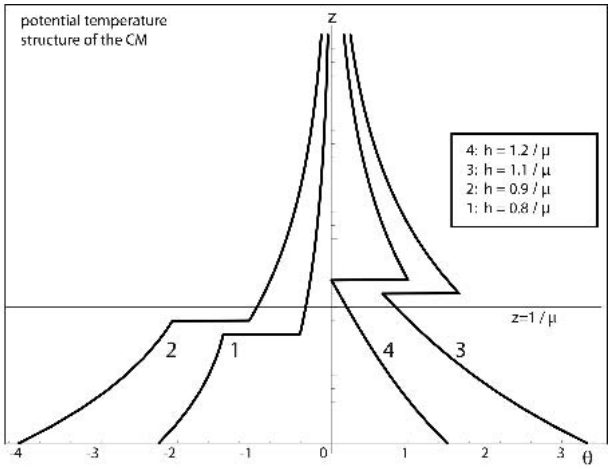

FIG. 1. The PT structure of the CM as a function of height z for different values of h and a positive value of the PV.

$$\left(\frac{\partial^2}{\partial t \partial z} - \frac{\partial \overline{U}}{\partial z}\frac{\partial}{\partial x}\right)\psi^{\mathrm{cm}}_{\theta} = \left(\frac{\partial \overline{U}}{\partial z}\frac{\partial}{\partial x}\right)\psi^{\mathrm{cm}}_{\mathrm{pv}}, \quad (\text{at } z = 0). \qquad (2.9)$$

Equation (2.9) states that there is a balance between processes related to surface PT and processes related to interior PV. It is easily verified that for $h < 1/\mu$, the advection of mean PT exceeds the tendency of the local perturbation PT due to ψ_{θ}. The forced balance of the three processes therefore gives a relation between the signs of interior PV and surface PT. More specifically, the sign of the PT must be of the opposite (same) sign of Q when $h < 1/\mu$ ($h > 1/\mu$). From the PV partitioning, it is clear that the amplitude of $\psi^{\mathrm{cm}}_{\theta}$ (and hence of ψ^{cm} itself) will get arbitrarily large when h approaches $1/\mu$, the steering level of the Eady edge wave. In this situation, the lhs of (2.9) becomes arbitrarily small, and the amplitude of $\psi^{\mathrm{cm}}_{\theta}$ increases to satisfy (2.9).

At $h = 1/\mu$ exactly, a linear resonance occurs because the PV anomaly and the edge wave move at the same speed and the lhs of (2.9) would vanish for a constant amplitude $\psi^{\mathrm{cm}}_{\theta}$. Straightforwardly solving the equations leads to the result of Thorncroft and Hoskins (1990):

$$\psi^{\mathrm{cm}}(x, z, t) = \psi^{\mathrm{cm}}_{\mathrm{pv}}(x, y, z, t) + \underbrace{\frac{Q\Lambda k}{\mu^2}te^{-\mu(z+h)}\cos\left[k\left(x - \frac{\Lambda}{\mu}t\right)\right]}_{\psi^{\mathrm{cm}}_{\theta,\mathrm{res}}(x,z,t)}, \qquad (2.10)$$

[1] Precise readers may convince themselves of the difference with the CM found in the existing literature on resonant modes. In Thorncroft and Hoskins (1990) as well as in Chang (1992) a factor $\exp(-\mu h)$ has been omitted erroneously.

with initial condition $\theta(z = 0, t = 0) = 0$ and where ψ_{pv}^{cm} is the same as in (2.6). The amplitude of $\psi_{\theta,res}^{cm}$ increases linearly in time and is a quarter of a wavelength out of phase with ψ_{pv}^{cm}, in agreement with calculations by Davies and Bishop (1994). This resonance exists for all values of the wavenumber k because the steering level of the Eady edge wave always lies in the physical domain.

3. Constructing a nonmodal PV basis

The discussion of the different modal solutions to the system of equations illustrates the importance of boundary conditions in PV dynamics. Although the dynamics of the CM itself is rather trivial (it is advected by the basic flow), the wind fields in the vicinity of the PV anomaly of the CM do not necessarily agree with standard PV thinking (Hoskins et al. 1985), especially for the near-resonant CM. The question arises whether or not in an analytical approach to the SV of the Eady model we can include the CMs without having to deal with the very large surface potential temperatures of the near-resonant CMs.

Equation (2.6) shows that the singular behavior of the CM near the steering level is caused by ψ_{θ}^{cm} only. This part of the CM exhibits the same exponential decay with height as an edge wave with the same wavelength. So it makes sense to build up the initial PV distribution of the SV with couplets consisting of one CM and one edge wave, which is superposed in such a way that the initial surface PT is zero (see Fig. 2 for a schematic representation). Due to the differences in propagation speed of edge wave and CM, a nonzero PT wave is generated as time increases. It is easily verified that, as a result of this superposition, the problem with the singularity is automatically postponed to $t=\infty$.

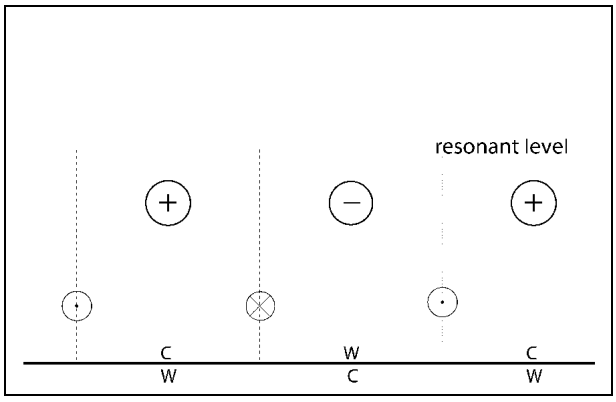

FIG. 2. Basis function in the PV basis. Here, ψ_{θ}^{cm} of a CM below the resonant level is masked by an edge wave with opposite amplitude. The PV anomalies are indicated by the encircled plus and minus signs. The wind fields due to the PV anomalies are represented by an encircled cross (northward) and dot (southward). The PT structure of the CM (edge wave) is indicated with the W and C signs just above (below) the surface.

It is known that the complete quasigeostrophic (QG) flow is determined by the distribution of interior PV and boundary PT (Hoskins et al. 1985). This implies that the CM edge wave couplets together with the edge waves can be used as building blocks to form a PV basis for perturbations with any initial distribution of interior PV and surface PT. Two advantages of this approach are immediately clear. First, the resonant mode is retained and second, the singular behavior of the near-resonant modes has been removed in a simple way. Additionally, the nonmodal approach allows a step-by-step construction of the SV. Instead of dealing with a general PV distribution in the SV, one may start with one PV building block in the initial perturbation and search for its optimal position, that is, the height that generates the largest surface cyclogenesis at the relevant time scale.

Definition of the singular vector

Singular vectors are constructed to produce optimal growth in some specified (vector) norm. In this paper we concentrate on the structure of the perturbation that generates the largest surface cyclogenesis and then a suitable choice seems to be the zonally integrated surface kinetic energy $E(t)$ (hereafter called the L norm). This L norm is not a proper vector norm but rather a vector seminorm that allows configurations with nonzero $\psi_{sv}(z)$ to have zero surface kinetic energy.[2] Given the meridional velocity $v = \partial\psi/\partial x$, $E(t)$ is computed as

$$E(t) = \int_0^{2\pi/k} \frac{v^2}{2}\, dx \bigg|_{z=0} \equiv \langle \psi(t), \psi(t) \rangle_L \bigg|_{z=0}, \tag{3.1}$$

where we have written the surface kinetic energy in terms of the correlation $\langle \psi(t), \psi(t) \rangle_L$ of the streamfunction with respect to the L norm. The ratio between the surface kinetic energy at initial and final time defines the finite-time growth factor:

$$\Gamma(t) = \frac{E(t)}{E(0)} \bigg|_{z=0}. \tag{3.2}$$

The next step is to vary the perturbation structure to optimize $\Gamma(t)$ for a given optimization time t. The perturbation structure that maximizes $\Gamma(t)$ is called the optimal perturbation or SV. In the next section we will calculate $\Gamma(t)$ for the streamfunction of one PV building block. As said before, at initial time this building block has PV at one particular level and zero PT at the surface. We will determine the position at which this initial PV anomaly generates the largest growth factor (3.2) for a given optimization time.

[2] For a vector seminorm $\|u\|^s = \|\mathbf{A} \cdot \mathbf{u}\| \geq 0$ (with $\|\cdot\|$ denoting the vector norm). In contrast with a proper vector norm, $\|u\|^s = 0$ does not imply that $u = 0$.

4. Optimal position of one PV anomaly

One obtains the streamfunction of one PV building block by adding an edge wave (2.4) to the CM [cf. (2.6)] in such a way that the surface PT of the perturbation is zero at initial time. This yields

$$\psi(x, z, t) = \psi_{\mathrm{pv}}^{\mathrm{cm}}(x, z, t) + \frac{Q}{\mu}\frac{e^{-\mu(z+h)}}{1-\mu h}\left\{\sin[k(x-\Lambda h t)] - \sin\left[k\left(x - \frac{\Lambda}{\mu}t\right)\right]\right\}. \quad (4.1)$$

A straightforward calculation gives the growth factor for this problem:

$$\Gamma(t) = \left\{\frac{1 + \mu^2 h^2 - 2\mu h \cos[k\Lambda(h - 1/\mu)t]}{(1-\mu h)^2}\right\}. \quad (4.2)$$

The growth factor is independent of the amplitude of the PV anomaly. Unfortunately, it is not possible to obtain the optimal height as a function of the optimization time analytically. Therefore (4.2) has been plotted in Fig. 3 for optimization times varying between 30 and 67 h. This figure shows that the maximum growth factor is obtained if the initial PV anomaly resides above the resonant level. For short optimization times the exact location of the CM is less important and maximal growth factors are obtained in a relatively broad regime above the resonant level. For larger optimization times this maximum moves asymptotically toward the resonant level and the band of optimal growth factors narrows. In the limit of infinite optimization time the maximum growth factor is obtained with an initial PV anomaly at the resonant level $h = 1/\mu$. The fact that for all times it is better to locate the initial PV anomaly not exactly at the resonant level shows that both resonance and unshielding play an important role in the finite-time optimization problem. In the next section we examine the importance of the various growth mechanisms during the development.

a. Projections of the SV streamfunction

Which of the possible growth mechanisms dominates the evolution of the SV? To answer this question we have calculated the different projections of the SV streamfunction. Morgan and Chen (2002) calculated projection coefficients for their modal-decomposed SV as well as for their PV–PT-decomposed SV. A similar analysis is presented below. The SV streamfunction ψ_{sv} is written as a sum of a PV and a PT part, $\psi_{\mathrm{sv}} = \psi_{\mathrm{pv}} + \psi_\theta$. The different growth mechanisms that play a role during the SV evolution are then just the different correlations appearing in the following expression:

$$\frac{\langle\psi_{\mathrm{pv}}, \psi_{\mathrm{pv}}\rangle_L}{\|\psi_{\mathrm{sv}}\|^2} + 2\frac{\langle\psi_{\mathrm{pv}}, \psi_\theta\rangle_L}{\|\psi_{\mathrm{sv}}\|^2} + \frac{\langle\psi_\theta, \psi_\theta\rangle_L}{\|\psi_{\mathrm{sv}}\|^2} = 1. \quad (4.3)$$

The subscript L indicates that we look at the different contributions to the surface kinetic energy (3.1), although the norm according to which the SV is calculated may be different. In (4.3) the first term on the left-hand side represents the contribution of the PV to the surface kinetic energy of the SV. Here, PV un-

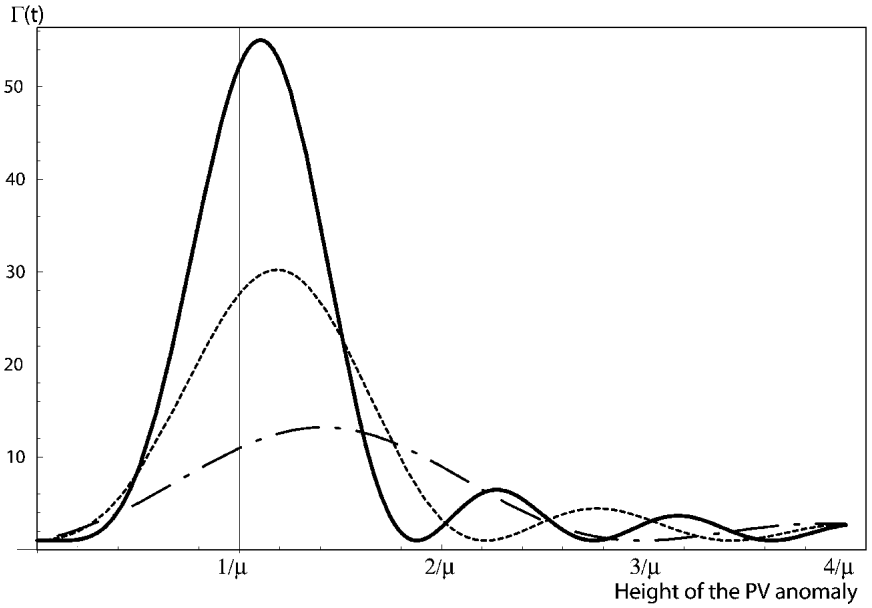

FIG. 3. Surface kinetic energy growth factor as a function of the height of the PV anomaly for different optimization times $t_{\mathrm{opt}} = 3.16$ (30 h; dash–dot), $t_{\mathrm{opt}} = 5.16$ (2 days; dashed), and $t_{\mathrm{opt}} = 7.16$ (67 h; full). The other parameters are $\Lambda = 1.0$, $k = 2.0$, and $S = 1.0$.

shielding does not occur and this gives $\langle \psi_{pv}, \psi_{pv} \rangle_L$ a constant, time-independent value. The second process is the unshielding of PV and PT. The last term on the left-hand side of (4.3) is the contribution of the resonance to the surface kinetic energy of the SV.

Figure 4 displays the evolution of the various projection coefficients for the $t_{opt} = 3.16$ (30 h) and $t_{opt} = 5.16$ (2 days) optimal building block. Initially, the SV completely projects on the PV part because there is zero surface PT. The surface winds due to the PV anomaly at optimal position then trigger a surface PT wave. This surface PT wave propagates with a slightly different propagation speed and we see that both resonance (dash–dot–dot) and PV–PT unshielding (full) contribute positively to the growth. Furthermore, we notice that for both optimization times the largest growth of the SV amplitude is caused by the resonance, and that unshielding of PV and PT plays a secondary role. This PV–PT-unshielding mechanism becomes important only if the optimization time is decreased. For optimization times smaller than about 13 h, PV–PT unshielding becomes the dominant growth mechanism.

In the next section we will elucidate the idea that PV–PT unshielding explains the location (i.e., above and not right at or below the resonant level) of the optimal PV building block.

b. The effect of PV–PT unshielding

The optimal position of the PV anomaly is found to be above the resonant level. One can show from (4.1) that the maximum of the surface PT wave (generated a quarter wavelength downwind of the PV maximum after $t = 0$) propagates with the mean speed of the PV anomaly and Eady edge wave. Therefore, if the PV resides above the steering level of the edge wave, this surface PT wave propagates toward the positive PV anomaly. On the other hand, the PT wave will propagate toward the negative PV anomaly if the PV lies below the steering level. In terms of PV thinking, this implies that in the former case the winds generated by the warm anomaly tend to add up with the winds due to PV, whereas the winds partially cancel in the latter case. This is illustrated schematically in Fig. 5.

For a given optimization time the situation with maximal possible surface kinetic energy is the one in which the net surface warm anomaly resides completely below the PV anomaly. This provides a theoretical upper limit for the height of the PV anomaly at

$$h = \frac{1}{\mu} + \frac{\pi}{k\Lambda t_{opt}}. \tag{4.4}$$

It turns out (see Fig. 3) that h_{opt} lies below the upper limit for all optimization times. This implies that at optimization time the SV has not yet reached maximal amplitude. For given h_{opt}, the maximal amplitude will be obtained at time $t = k\Lambda/[\pi(h_{opt} - 1/\mu)]$. The fact that the actual optimal height is below the upper limit for all optimization times illustrates the dominance of the resonance. Unshielding of ψ_{pv} and ψ_θ occurs more rapidly if the PV is far away from the steering level. On the contrary, the resonance effect of a growing ψ_θ is stronger if the PV is located closer to the steering level. The optimal position is somewhere in between and depends on the optimization time.

c. Summary

To conclude this section, we present a short summary of the results. It has been shown that resonance is the most important growth mechanism for one optimal building block. Unshielding of PV and PT has a secondary effect and generates significant additional growth only for small optimization times. For large optimization times virtually all growth is explained by the resonance.

In the present study the optimization procedure maximizes surface kinetic energy at optimization time given the constraint that the initial surface kinetic en-

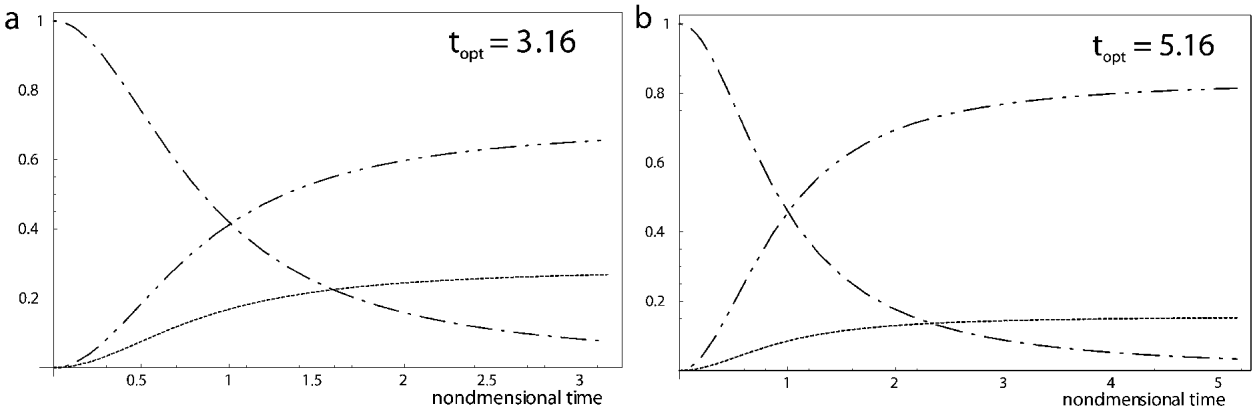

FIG. 4. The time evolution of the projection coefficients for the (a) $t_{opt} = 3.16$ (30 h) and (b) $t_{opt} = 5.16$ (2 days) optimal building block. Shown are $\langle \psi_{pv}, \psi_{pv} \rangle_L / \|\psi_{sv}\|^2$ (dash–dot), $2\langle \psi_{pv}, \psi_\theta \rangle_L / \|\psi_{sv}\|^2$ (dotted), and $\langle \psi_\theta, \psi_\theta \rangle_L / \|\psi_{sv}\|^2$ (dash–dot–dot).

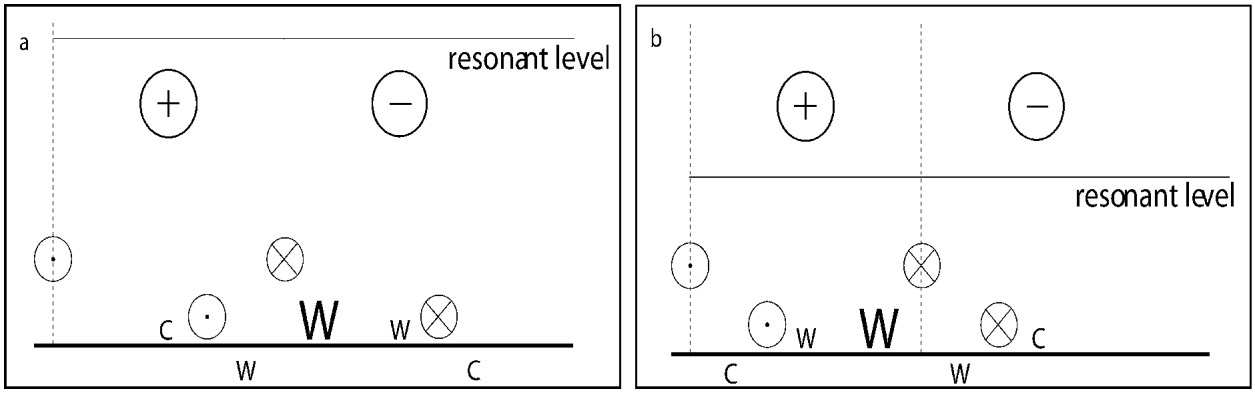

FIG. 5. Schematic evolution of a CM edge wave couplet (a) below and (b) above the resonant level. The large W indicates the location of the net surface warm anomaly (the lower encircled cross and dot are the wind fields around this net warm anomaly). Other symbols are the same as in Fig. 2.

ergy is unity. A different approach would be to study the sensitivity of the system to a PV anomaly of a given (i.e., unit) initial amplitude. Optimizing the surface kinetic energy under this different constraint will obviously produce different results. In this case it is more favorable to locate the PV in the lower atmosphere (to produce a larger surface kinetic energy in the initial perturbation). For small optimization times this alternative optimization procedure produces PV located near the surface, whereas for larger optimization time the PV approaches the steering level from below. In terms of the growth factor (3.2), however, these low-level PV anomalies are not optimal.

Although the baroclinic development of one PV building block has some realistic features, the singular character of the PV anomaly must be considered highly unrealistic. It is known that a more realistically shaped initial PV distribution will be affected by smoothing effects. For the semi-infinite Eady model, Chang (1992) mentions that nonresonance effects will dominate the dynamics in any finite-size continuous sample. Chang's study does not answer the question of whether this "finite-size" effect will enhance or diminish the perturbation growth. This will be discussed in the next section. By adding more PV building blocks to the initial perturbation, we will study the impact of PV unshielding on the growth of the SV.

5. Toward a general PV distribution

What happens when more PV building blocks are allowed in the initial perturbation and one optimizes the initial structure to produce a maximal growth factor? It is easy to verify that a growth factor based on the surface kinetic energy runs into problems because the streamfunction of two (or more) PV anomalies may cancel at one particular level. As a consequence, any optimization algorithm generates zero initial surface kinetic energy in the search for an optimal growth factor $\Gamma(t)$. Any nonzero final surface kinetic energy will produce an (almost) infinite growth factor.

The problem is even worse. By looking at the structure of the initial PV anomaly and its mathematical representation $\psi_{\text{pv}}^{\text{cm}}$ in (2.6), it is clear that for a suitable choice of amplitudes and initial phase difference, the total streamfunction associated with two PV anomalies may vanish completely below the lower PV anomaly. To solve the problem one needs to integrate over a domain that includes at least the levels where the PV anomalies reside. This may well be the reason that a total kinetic energy norm (which is a proper vector norm unlike the surface kinetic energy) is used in most numerical simulations (Farrell 1989; Morgan 2001; Morgan and Chen 2002; Kim and Morgan 2002). In this study an integration height of 4 times the Rossby height has been chosen. We have experimentally verified that the PV perturbations at the top levels have a negligible contribution to structure and the evolution of the SV at the surface.

The results for the one-couplet problem carry over when changing to a total kinetic energy norm. In this norm, the optimal height of the PV anomaly is located closer to the resonant level for all optimization times (cf. with Fig. 3). When the number of PV anomalies in the initial perturbation increases, the mathematical expression for the growth factor gets cumbersome. Fortunately, a straightforward technique exists to solve the optimization problem numerically. This method is normally used in combination with a modal analysis, but is easily modified to the nonmodal case we adopt here. This technique is discussed in appendix A. When determining the total kinetic energy numerically one needs to choose representative levels to calculate the energy. A suitable choice followed here is to calculate the energy at the same levels as where the PV anomalies reside. In appendix B, we briefly comment on another reasonable possibility (in between the PV anomalies) yielding unphysical results.

a. Results for two PV anomalies

When we have two PV anomalies residing at two of the M possible interior levels, say h_1 and h_2, the eigenfunction matrix $\mathbf{X}(t)$ defined in Eq. (A.1) becomes $2 \times M$ dimensional. For given h_1 and h_2, the optimal structure is calculated using Eq. (A.4) and a total kinetic energy norm. Also, h_1 and h_2 are varied in height to obtain the global maximum in parameter space (h_1, h_2). In Fig. 6 we have plotted the growth factor for nondimensional optimization time $t_{\text{opt}} = 5.16$ (2 days) as a function of the height h_2 retaining h_1 at its global optimum. Again we see a rather sharp peak above the resonant level. It may be verified that both PV anomalies lie above the resonant level and below the maximum level as defined by (4.4) again, similar to the SV constructed with one PV anomaly.

Figure 7 displays the evolution of the SV streamfunction. The PV anomalies reside at optimal positions ($z = 0.566$ and at $z = 0.642$) and are almost completely out of phase initially. Therefore, the total streamfunction vanishes except in a narrow region around the positions of the anomalies (Fig. 7a). Comparing Figs. 7a and 7c, we see that initially the SV completely projects on the PV part. As time increases, the PV anomalies disperse, and the streamfunction reaches the surface (Figs. 7h and 7i). The surface winds then start to advect the background gradient in PT and a surface PT wave is generated (Figs. 7n–r). The surface PT wave quickly amplifies because of the resonance between the PV anomalies and the edge waves. At the optimization time $t = 5.16$, the surface PT wave has obtained a large amplitude and most of the surface winds in this stage are attributable to the surface temperature perturbation (cf. Figs. 7l and 7r). The growth factor, now defined with respect to the total kinetic energy, reaches the value of 83.5 at the optimization time. Notice that the two PV anomaly problem has not evolved completely into a vertical PV tower at $t = t_{\text{opt}}$.

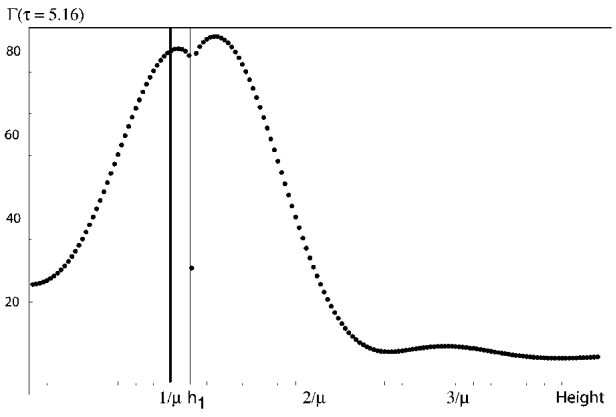

FIG. 6. Height dependence of Γ for $t_{\text{opt}} = 5.16$. Here, h_1 is fixed at its optimal level (indicated by the thin line) and h_2 is varied to show the height dependence of the optimal solution. The isolated minimum for h_2 just above the resonant level is the situation where both PV anomalies reside at the same height and PV unshielding does not occur.

To get a more quantitative insight into the surface development, we have plotted the evolution of the projection coefficients (4.3) of the $t_{\text{opt}} = 5.16$ SV in Fig. 8. In this case PV–PT unshielding contributes negatively to the surface growth of the SV in the initial stages. Contrast this with Fig. 4 where PV–PT unshielding was positive during the complete evolution. The resonance still dominates the surface development at the final time.

b. Results for M PV anomalies

To be complete, we present here the result for $M = 40$, which is a simulation of the continuous problem. Again $t_{\text{opt}} = 5.16$ and the SV is constructed for the total kinetic energy norm. The evolution of the SV toward $t = t_{\text{opt}}$ and its underlying PV and PT part are displayed in Fig. 9. For the interior, PV unshielding has become the dominant mechanism in the complete evolution of the SV toward $t = 5.16$. We start off with a streamfunction structure that is tilted rather upshear with height and that is concentrated in a narrow region just above the resonant level (see Figs. 9a and 10a). Once the streamfunction has reached the surface (Fig. 9c) a PT wave is rapidly developing (Figs. 9p–r). At optimization time the streamfunction attributable to the PV anomalies is almost barotropic (Fig. 9l). In contrast with the two-couplet SV, the SV with M couplets form an almost vertical PV structure at optimization time. Figure 10b shows this towering of PV. Only the few top levels are out of phase. This is because these top levels take into account the average influence of all levels above and they therefore may be positioned (slightly) out of phase.

Let us now turn to the surface dynamics. Figure 11 shows the evolution of the different projection coefficients (4.3) for two different optimization times. Something unexpected seems to be happening at the surface in the initial stages of the development (Fig. 11a). However, a close inspection shows that the projection coefficients explode because ψ_{sv} at $z = 0$ almost vanishes at this point in time. That is, the rapid surface cyclogenesis occurring roughly after $t = 1$ is preceded by an initial surface cyclolysis. This is perfectly possible because we have chosen total kinetic energy as an optimization norm. After this initial weakening of the surface winds, the resonance clearly takes over the surface development at $t \sim 4.2$ leading to a total kinetic energy growth factor of 622.0 at optimization time. Prior to $t \sim 4.2$, PV unshielding dominates the evolution. PV–PT unshielding contributes negatively to the surface development during almost the complete time evolution. Increasing the optimization time (Fig. 11b) to 4 days leads to similar results for the surface development as we saw before in the case with one or two PV anomalies (Fig. 8); resonance becomes increasingly more important.

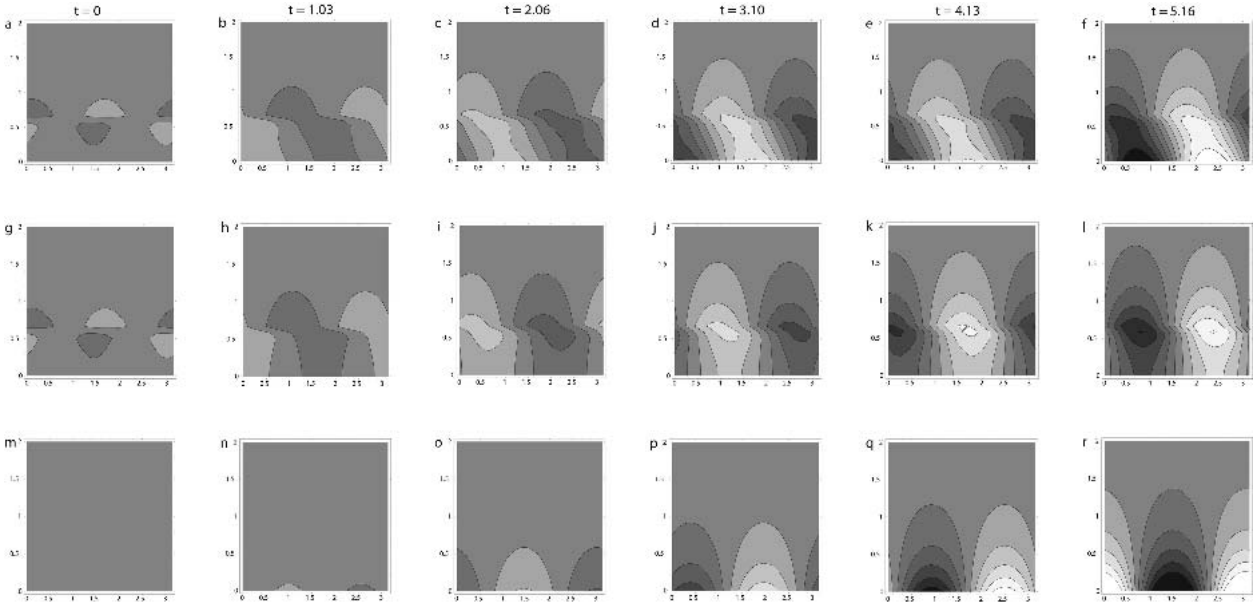

FIG. 7. Evolution of the streamfunction of the two-couplet SV for $t_{opt} = 5.16$ and $k = 2.0$. Displayed are (a)–(f) the total SV streamfunction, (h)–(l) the part of ψ that is associated with the PV only, and (m)–(r) the part of ψ that is associated with the boundary PT only. At the optimization time, the growth factor has reached a value of 83.5. Range of contours is (−1, 1).

Yet another way to illustrate the importance of resonance in the general problem is to consider the distribution of PV in the vertical. In Fig. 12, we displayed the amplitudes of the PV at specific levels for the $t_{opt} = 5.16$ (2 days) and $t_{opt} = 10.32$ (4 days) SV. These figures share similarities with Fig. 3, although in Fig. 3 we have plotted the growth factor as function of the height of one PV anomaly. We see that for $t_{opt} = 5.16$ the largest amplitudes of PV are typically observed in a rather wide domain above the resonant level. This is in line with the observation that during the complete time evolution the interior SV is dominated by growth due to PV superposition and not resonance. The resonance effect is already more important for a doubled optimization time. In this case there is a rather sharp peak in a small region above the resonant level, and we expect that an even more significant part of the development will be due to resonance. This is confirmed by looking at Fig. 11b.

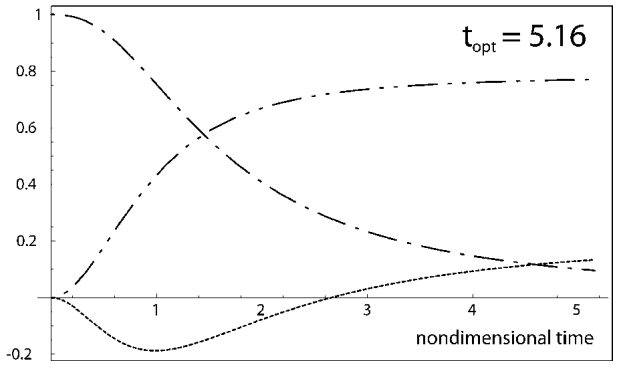

FIG. 8. The time evolution of the projection coefficients for the $t_{opt} = 5.16$ SV with two PV anomalies in the initial perturbation. Displayed are $(\langle\psi_{pv},\psi_{pv}\rangle_L/\|\psi_{sv}\|^{-2})|_{z=0}$ (dash–dot), $(2\langle\psi_{pv},\psi_\theta\rangle_L|\psi_{sv}|^{-2})|_{z=0}$ (dotted), and $(\langle\psi_\theta,\psi_\theta\rangle_L/\|\psi_{sv}\|^{-2})|_{z=0}$ (dash–dot–dot). Remember that the SV itself is calculated with respect to the total kinetic energy norm.

6. Concluding remarks

In this paper we have discussed how resonance and potential vorticity (PV) unshielding dominate the evolution of the SV of the Eady model without an upper rigid lid. The normal modes of this model are baroclinically stable. However, one member of the set of continuum modes (CMs) produces a linear resonance. This resonating CM is left out in many existing studies on optimal perturbations. We have used the PV perspective to construct a set of nonmodal basis functions. These basis functions initially have PV at some specific level and zero surface potential temperature (PT). By meridionally advecting the PT of the basic state, a surface PT wave is generated as time increases. The surface PT wave and the interior PV wave will interact through the mean flow.

The nonmodal basis allowed a number of initial value experiments, in which the number of interior PV anomalies (PV building blocks) in the initial perturbation is gradually increased. Gradually increasing the complexity of the initial perturbation structure has the advantage that different growth mechanisms can be more easily distinguished than would be the case in a

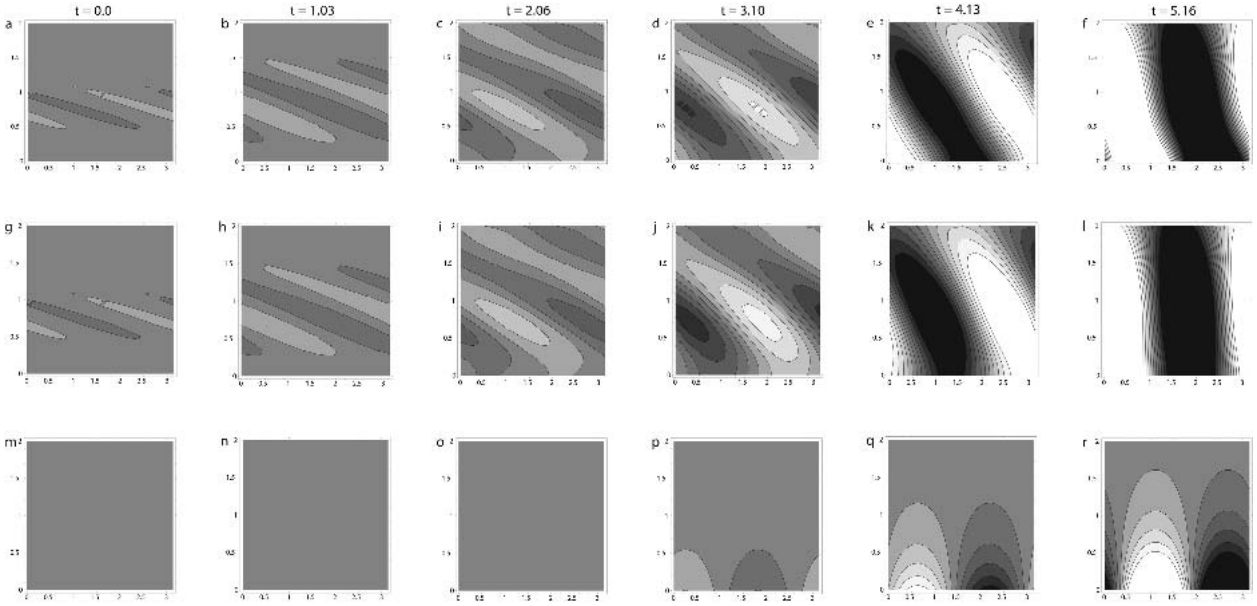

FIG. 9. Evolution of the streamfunction of the ($M = 40$)-couplet SV for $t_{opt} = 5.16$ and $k = 2.0$. Displayed are (a)–(f) the total SV streamfunction, (g)–(l) the part of ψ that is associated with the PV only, and (m)–(r) the part of ψ that is associated with the surface PT only. At optimization time, the growth factor has reached the value 622.0. Range of contours is $(-2, 2)$.

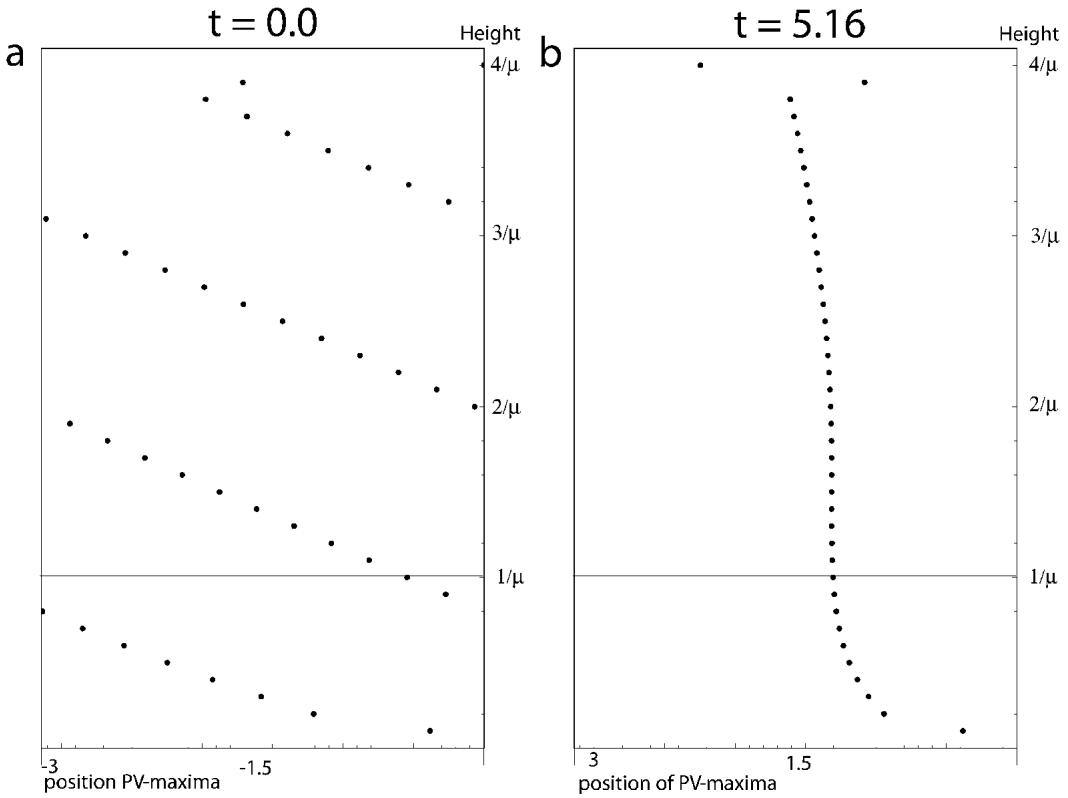

FIG. 10. (a) Initial and (b) final PV configuration for the $t_{opt} = 5.16$ SV.

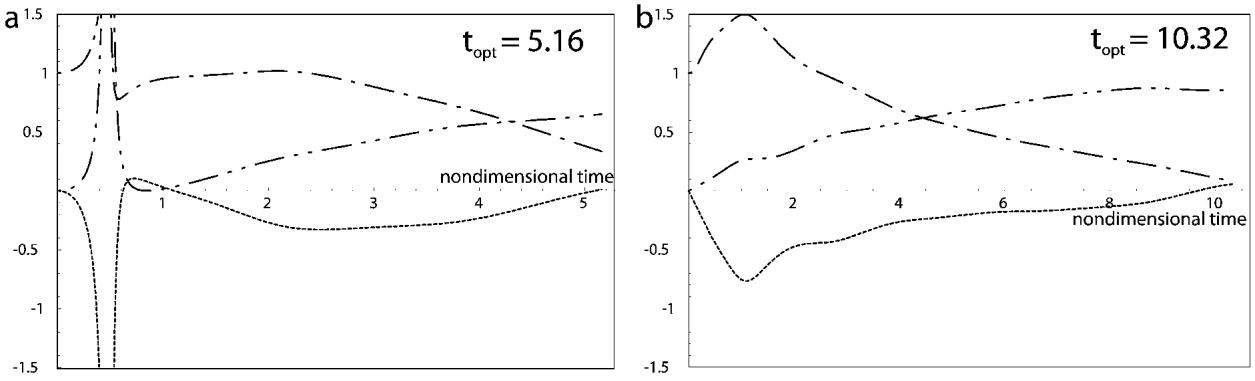

FIG. 11. The time evolution of the projection coefficients for (a) the $t_{opt} = 5.16$ and (b) $t_{opt} = 10.32$ SV with $M = 40$ PV anomalies. Shown are $(\langle\psi_{pv},\psi_{pv}\rangle_L/\|\psi_{sv}\|^{-2})|_{z=0}$ (dash–dot), $(2\langle\psi_{pv},\psi_\theta\rangle_L\|\psi_{sv}\|^{-2})|_{z=0}$ (dotted), and $(\langle\psi_\theta,\psi_\theta\rangle_L/\|\psi_{sv}\|^{-2})|_{z=0}$ (dash–dot–dot).

completely general analysis. These mechanisms are PV unshielding, PV–PT unshielding, and resonance (a growing surface PT wave). Frequently encountered problems with the near singular behavior of the CMs near one Rossby height are avoided in this approach.

Results of the experiments indicate that when there is only one PV anomaly in the interior, the optimal position of this PV anomaly is found in a region above the steering level of the Eady edge wave. The largest part of the baroclinic growth is caused by the resonance between the PV anomaly and the surface edge wave. This resonance produces a rapidly growing surface PT wave. We have showed that above the steering level of the surface edge wave, PV–PT unshielding contributes additionally to the growth due to the resonance, but that this effect is only important for small optimization times.

PV unshielding does not occur for an SV constructed from one PV anomaly. Therefore, to include PV unshielding as a third growth mechanism, more PV anomalies were added in the initial perturbation. When the number of PV anomalies is more than two, PV unshielding becomes the dominant growth mechanism for the interior. This is to be contrasted with the surface development for which resonance remains the dominant growth mechanism. The PV distribution of the SV approaches the steering level of the edge wave from above when optimization time is increased. This illustrates the enhanced importance of resonance for long optimization times as compared to short optimization times.

The surface edge wave can grow as a result of interaction with PV modes close to the resonant level and also as a result of interaction with the upper-boundary edge mode. In this study the upper edge mode is not present. To estimate its contribution, we have computed the growth factor due to baroclinically interacting edge modes (by adding a rigid lid at 10 km) for the $k = 2$ case considered in this study. We find growth factors that are substantially smaller than the growth

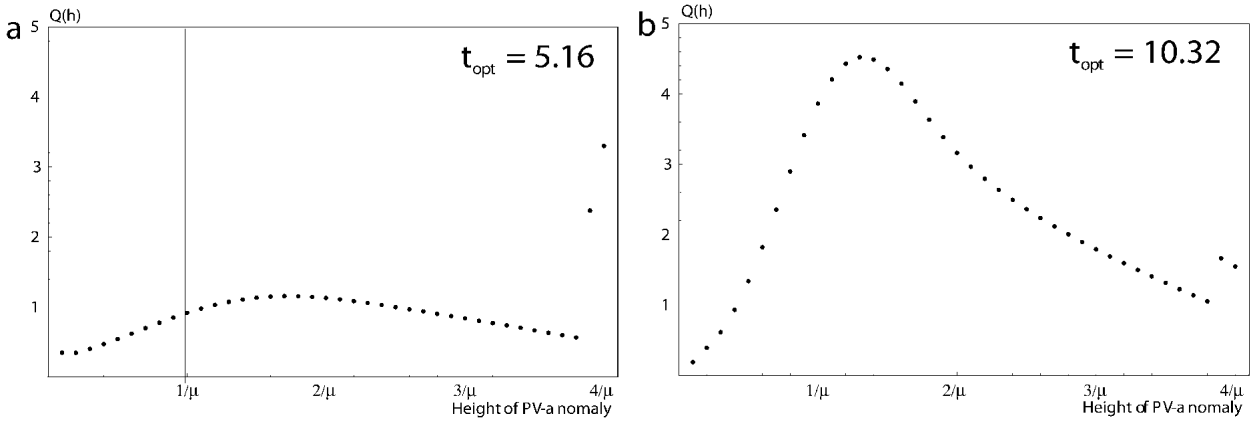

FIG. 12. Amplitudes of the PV maxima for (a) the $t_{opt} = 5.16$ SV and (b) $t_{opt} = 10.32$ SV. The anomalous large amplitude of the PV at the two topmost levels is the effect of truncating the vertical domain at $z = 4/\mu$, and in some sense summarized the mean effect of all modes above that level.

factor due to the resonance effect studied in this paper.[3] So the resonance effect seems to be a more efficient form of baroclinic instability if short optimization times are considered.

A possible generalization of the present study is related to the choice of norm. We have chosen equal norms at the initial and final time. Another interesting possibility is to optimize for a total kinetic or total quasigeostrophic energy norm at the initial time and a surface kinetic energy norm at the final time. We are currently investigating the consequences of this different choice of norm for the resonance described in the paper.

Acknowledgments. The authors thank Dr. A. J. van Delden for valuable discussions and two anonymous reviewers for their comments and suggestions.

APPENDIX A

Numerical Determination of the SV

The standard numerical approach to the optimization problem divides the atmosphere in M horizontal levels. The discretized, linearized dynamical operator yields M eigenvectors, which describe the modal structures supported by the basic flow. The problem with the large amplitude of the CM near the resonant level is removed by rescaling the CM to unit amplitude in some physical norm (Morgan and Chen 2002). In this way, the resonant mode is systematically excluded from the continuous spectrum and only near-resonant modes are retained. Instead of using the conventional normalized modal basis, we use the more physically oriented PV basis. For each level $h_i \geq 0$, Eq. (4.1) describing the time evolution of a PV anomaly at height h_i defines an eigenfunction $\psi(x, z, t; h_i)$ in the space of all possible perturbation structures. This eigenfunction is represented by an M-dimensional vector $\boldsymbol{\psi}(x, z, t; h_i)$ with coefficients $[\boldsymbol{\psi}(x, z, t; h_i)]_j = \psi(x, z_j, t; h_i)$. With these eigenfunctions one constructs the $M \times M$ matrix $\mathbf{X}(t)$ with the following coefficients:

$$[\mathbf{X}]_{ij}(t) := \psi(x, z_i, t; h_j). \tag{A.1}$$

Any perturbation streamfunction $\boldsymbol{\psi}_{\text{arb}}$ is represented by an M-dimensional state vector. This state vector can be decomposed in the complete set of basis functions with appropriate projection coeffients of a_i:

$$\boldsymbol{\psi}_{\text{arb}}(x, z, t) = \sum_{j=1}^{M} a_j \boldsymbol{\psi}_j(x, z, t; h_j) = \mathbf{X}(t) \cdot \mathbf{a}. \tag{A.2}$$

With the matrix of basis functions and the choice of the norm, the numerical determination of the SV is straightforward. The functional to be maximized is known since the work of Borges and Hartmann (1992). In the present PV basis it reads as[1]

$$\theta(\mathbf{a}) = \mathbf{a}^{\text{H}} \cdot [\mathbf{X}(t)^{\text{H}} \cdot \mathbf{X}(t)] \cdot \mathbf{a} - \lambda^2 \{\mathbf{a}^{\text{H}} \cdot [\mathbf{X}(0)^{\text{H}} \cdot \mathbf{X}(0)] \cdot \mathbf{a} - 1\}, \tag{A.3}$$

with $\mathbf{A}^{\text{H}}$ meaning the conjugate transpose of the object $\mathbf{A}$. Here the streamfunction variance norm (L2 norm) is used. Setting the first variation of $\theta(\mathbf{a})$ with respect to $\mathbf{a}$ equal to zero, one may verify that the optimal perturbation structure is given by the eigenfunction corresponding to the largest eigenvalue $\lambda^2 = \lambda^2_{\text{max}}$ of the following eigenvalue problem:

$$[\mathbf{X}(0)^H \cdot \mathbf{X}(0)]^{-1} \cdot [\mathbf{X}(t)^H \cdot \mathbf{X}(t)]\mathbf{a} = \lambda^2 \mathbf{a}, \tag{A.4}$$

and $\boldsymbol{\psi}(0)$ is given by $\mathbf{X}(0)\mathbf{a}$. For a fixed horizontal wavenumber, the L2 norm and the total kinetic energy norm are closely related. The growth factor defined in (3.2) is equivalent with λ^2_{max} above if, instead of surface kinetic energy, the total kinetic energy is used. Here we have approximated the integral of kinetic energy in the vertical by a sum over the kinetic energies at the levels. Alternatively, one may wish to compute the entries in $\mathbf{X}(t)^{\text{H}}\,\mathbf{X}(t)$ analytically similar to the approach of Fischer (1998). In this way the SV is determined completely analytically.

The above eigenvalue problem can be easily generalized to optimize for different norms, such as total quasigeostrophic energy norm or potential enstrophy norm (Kim and Morgan 2002). The solution to the eigenvalue problem determines the complex valued projection vector $\mathbf{a}$, and hence the amplitude and phases of the PV anomalies (CM-edge wave couplets) and the surface PT of the initial perturbation.

APPENDIX B

Spurious Modes for Different Discretizations

In section 5 we used a particular discretization for the calculation of the total kinetic energy. The energy is calculated at the same levels as where the PV is specified. Although this is a standard approach and is done in most numerical studies, there is no a priori reason why one should use this discretization. In this appendix, the energy is calculated at levels in between the levels at which the PV is specified. We study the M-couplet problem, with all further specifications and assumptions equal to the ones of section 5. Figure B1 displays the results for the phases of the initial PV distribution. The initial and final phases show a rather dramatic difference when compared to the initial and final phases of Fig. 10. Instead of being upshear tilted, there is now a phase distribution where all subsequent couplets lie one-half of a wavelength out of phase. That is, they

[3] A standard normal mode analysis for $k = 2$ and a rigid lid at $z = 10$ km gives a growth rate of the unstable normal mode $kc_i = 0.27$. For the nondimensional time $t_{\text{opt}} = 5.16$ this gives a growth factor due to normal mode instability only $\Gamma = \exp(2kc_i t_{\text{opt}}) = 16.6$.

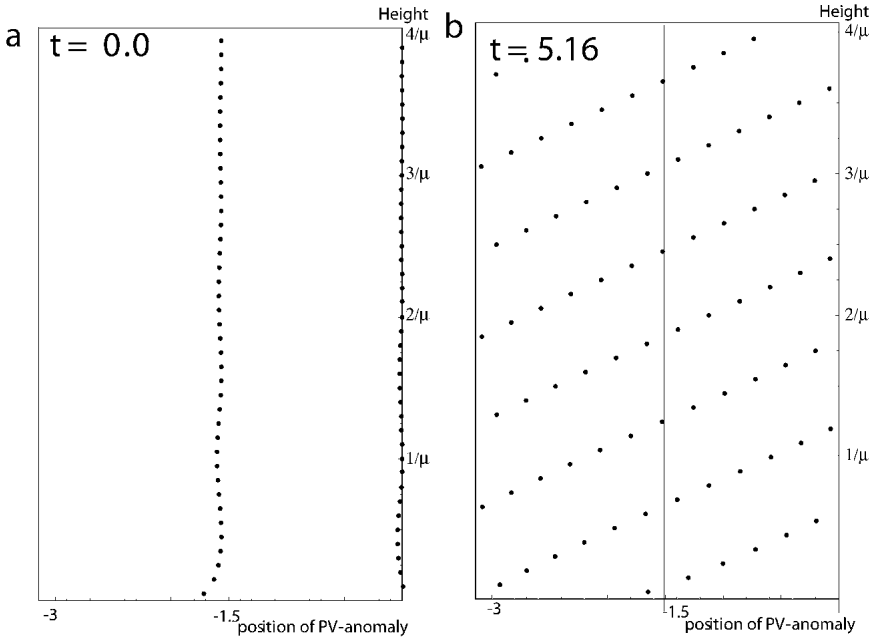

FIG. B1. (a) Initial and (b) final position of the PV maxima for the $t_{opt} = 5.16$ SV calculated with a different method.

competely mask each other, similar to the result of the two-couplet problem in section 5. Why has the SV chosen this "unphysical" structure? The reason is that the streamfunction in between two PV anomalies is almost zero when those modes are one-half of a wavelength out of phase. Therefore, by choosing the structure in Fig. B1, the system minimized the initial kinetic energy very effectively. To ensure unit initial kinetic energy, the amplitudes of PV at the levels increase enormously. This emphasizes the fact that one has to be careful in calculating the kinetic energy at levels h_i, which are representative for the whole layer $|h_i - \delta h|$, where $\delta h = \frac{1}{2}|h_i - h_{i+1}|$.

REFERENCES

Badger, J., and B. J. Hoskins, 2001: Simple initial value problems and mechanisms for baroclinic growth. *J. Atmos. Sci.,* **58,** 38–49.

Bishop, C. H., and E. Heifetz, 2000: Apparent absolute instability and the continuous spectrum. *J. Atmos. Sci.,* **57,** 3592–3608.

Borges, M. D., and D. L. Hartmann, 1992: Barotropic instability and optimal perturbations of observed nonzonal flows. *J. Atmos. Sci.,* **49,** 335–353.

Chang, E. K. M., 1992: Resonating neutral modes of the Eady model. *J. Atmos. Sci.,* **49,** 2452–2463.

Davies, H. C., and C. H. Bishop, 1994: Eady edge waves and rapid development. *J. Atmos. Sci.,* **51,** 1930–1946.

Eady, E. T., 1949: Long waves and cyclone waves. *Tellus,* **1,** 33–52.

Farrell, B. F., 1982: The initial growth of disturbances in a baroclinic flow. *J. Atmos. Sci.,* **39,** 1663–1686.

——, 1984: Modal and non-modal baroclinic waves. *J. Atmos. Sci.,* **41,** 668–673.

——, 1988: Optimal excitation of neutral Rossby waves. *J. Atmos. Sci.,* **45,** 163–172.

——, 1989: Optimal excitation of baroclinic waves. *J. Atmos. Sci.,* **46,** 1193–1206.

Fischer, C., 1998: Linear amplification and error growth in the 2D Eady problem with uniform potential vorticity. *J. Atmos. Sci.,* **55,** 3363–3380.

Hakim, G. J., 2000: Role of nonmodal growth and nonlinearity in cyclogenesis initial-value problems. *J. Atmos. Sci.,* **57,** 2951–2967.

Hoskins, B. J., M. E. McIntyre, and A. W. Robertson, 1985: On the use and significance of isentropic potential vorticity maps. *Quart. J. Roy. Meteor. Soc.,* **111,** 877–946.

Kim, H. M., and M. C. Morgan, 2002: Dependence of singular vector structure and evolution on the choice of norm. *J. Atmos. Sci.,* **59,** 3099–3116.

Morgan, M. C., 2001: A potential vorticity and wave activity diagnosis of optimal perturbation evolution. *J. Atmos. Sci.,* **58,** 2518–2544.

——, and C. C. Chen, 2002: Diagnosis of optimal perturbation evolution in the Eady model. *J. Atmos. Sci.,* **59,** 169–185.

Mukougawa, H., and T. Ikeda, 1994: Optimal excitation of baroclinic waves in the Eady model. *J. Meteor. Soc. Japan,* **72,** 499–513.

Orr, W., 1907: Stability or instability of the steady-motions of a perfect liquid. *Proc. Roy. Irish Acad.,* **27,** 9–138.

Pedlosky, J., 1964: An initial value problem in the theory of baroclinic instability. *Tellus,* **16,** 12–17.

Rotunno, R., and M. Fantini, 1989: Petterssen's "Type B" cyclogenesis in terms of discrete, neutral Eady modes. *J. Atmos. Sci.,* **46,** 3599–3604.

Thorncroft, C. D., and B. J. Hoskins, 1990: Frontal cyclogenesis. *J. Atmos. Sci.,* **47,** 2317–2336.